C.E. SACLAY
DSM

SERVICE D'ASTROPHYSIQUE

SAP 1996/37 JUIN 1996

PROBING THE INITIAL CONDITIONS OF STAR FORMATION : THE STRUCTURE OF THE PRESTELLAR CORE L1689B

DAPNIA

P.ANDRE, D.WARD-THOMPSON, F.MOTTE

Le DAPNIA (Département d'Astrophysique, de physique des Particules, de physique Nucléaire et de l'Instrumentation Associée) regroupe les activités du Service d'Astrophysique (SAp), du Département de Physique des Particules E1émentaires (DPhPE) et du Département de Physique Nucléaire (DPhN).

Adresse : DAPNIA, Bâtiment 141
CEA Saclay
F -91191 Gif-sur-Yvette Cedex

A&A manuscript no.
(will be inserted by hand later)

Your thesaurus codes are:
(08.05.1; 09.08.1)

ASTRONOMY
AND
ASTROPHYSICS
10.7.1996

Probing the initial conditions of star formation: The structure of the prestellar core L1689B

P. André[1⋆], D. Ward-Thompson[2⋆⋆], F. Motte[1,3]

[1]CEA, DSM, DAPNIA, Service d'Astrophysique, C.E. Saclay, F-91191 Gif-sur-Yvette Cedex, France
[2]Royal Observatory, Blackford Hill, Edinburgh EH9 3HJ, UK
[3]Observatoire de Grenoble, BP 53, F-38041 Grenoble Cedex 9, France

Received 23 February 1996 / accepted 3 April 1996

Abstract. In a recent JCMT submillimeter study, Ward-Thompson et al. (1994) obtained the first dust continuum maps of five low-mass dense cores among the sample of starless ammonia cores from Myers and colleagues. Here, we present the results of new 1.3 mm continuum mapping observations for one of these cores, L1689B, taken with the IRAM 30-m telescope equipped with the 7–channel and 19–channel MPIfR bolometer arrays. The new 1.3 mm data, which were obtained in the 'on-the-fly' scanning mode, have better angular resolution and sensitivity than the earlier 800 μm data, reaching an rms noise level of ~ 3 mJy/13″beam. Our IRAM map resolves L1689B as an east-west elongated core of deconvolved size 0.045 pc $\times$ 0.067 pc (FWHM), central column density $N_{H_2} \sim 1.5 \times 10^{22}$ cm^{-2}, and mass $M_{FWHM} \sim 0.6\ M_\odot$, in good agreement with our previous JCMT estimates. We confirm that the radial column density profile $N(\theta)$ of L1689B is not consistent with a single power law with angular radius θ but flattens out near its centre. Comparison with synthetic model profiles simulating our 'on-the-fly' observations indicates that $N(\theta_{maj}) \propto \theta_{maj}^{-0.2}$ for $\theta_{maj} \leq 25''$ and $N(\theta_{maj}) \propto \theta_{maj}^{-1}$ for $25'' < \theta_{maj} \leq 90''$, where θ_{maj} is measured along the major axis of the core. The observed mean profile is *not* consistent with a simple Gaussian source, being flatter than a Gaussian in its outer region. However, the profile measured along the minor axis of L1689B is significantly steeper and apparently consistent with a Gaussian 'edge' in the north-south direction. The mass, radius, and density of the relatively flat central region are estimated to be $\sim 0.3\ M_\odot$, ~ 4000 AU, and $\sim 2 \times 10^5$ cm^{-3}, respectively.

The mass of L1689B and its large (> 30) density contrast with the surrounding molecular cloud indicate that it is not a transient structure but a self-gravitating prestellar core. The flat inner profile and other measured characteristics of L1689B are roughly consistent with theoretical predictions for a magnetically-supported, flattened core either on the verge of collapse or in an early phase of dynamical contraction. In this case, the mean magnetic field in the central region should be $\lesssim 80\ \mu$G, which is high but not inconsistent with existing observational constraints. Alternatively, the observed core structure may also be explained by equilibrium models of primarily thermally supported, self-gravitating spheroids interacting with an external UV radiation field.

The present study supports the conclusions of our previous JCMT survey and suggests that, in contrast with protostellar envelopes, most pre-stellar cores have flat inner density gradients which approach $\rho(r) \propto r^{-2}$ only beyond a few thousand AU. This implies that, in some cases at least, the initial conditions for protostellar collapse depart significantly from a singular isothermal sphere.

Key words: interstellar medium: dust – formation of stars

1. Introduction

Despite recent observational and theoretical progress, the initial conditions for protostellar collapse remain poorly known. The earliest protostellar stage observed so far appears to be the main infall/outflow phase of star formation, in which a central hydrostatic protostar has formed, but not yet accreted the majority of its final main-sequence mass. At this stage, most of the mass is still in the form of a dense circumstellar envelope. The best observational candidates for this phase are the Class 0 objects recently identified by André, Ward-Thompson & Barsony (1993 – hereafter AWB93; see André 1995 for a review). The Class 0 stage is presumably preceded by

Send offprint requests to: P. André
⋆ email: andre@sapvxg.saclay.cea.fr
⋆⋆ email: dwt@roe.ac.uk

a very brief isothermal collapse phase in which no hydrostatic core is present (e.g., Boss & Yorke 1995). Observationally, however, this isothermal phase remains elusive (e.g., Chini et al. 1993; Bontemps, André, & Ward-Thompson 1995).

Prior to these protostellar stages, the pre-protostellar phase of star formation (hereafter referred to as the pre-stellar phase for brevity) may be defined as a phase in which a gravitationally bound fragment has formed in a molecular cloud, and evolves towards progressively higher degrees of central condensation, eventually leading to protostellar collapse. Observationally, it is by comparing the structure of pre-stellar cores with that of Class 0 protostars that one may hope to constrain the physical conditions at the onset of protostellar collapse.

Many low angular resolution, molecular line surveys of dense cloud cores have been carried out, leading to the identification of a large number of potential low-mass star-forming sites (e.g. Myers, Linke & Benson 1983 – hereafter MLB; Benson & Myers 1989 – hereafter BM89 – and references therein). Roughly half of the 'Myers' dense cores have associated IRAS point sources, the other half being designated 'starless' (e.g., Beichman et al. 1986). Most of these starless cloud cores are gravitationally virialized (see Myers 1983) and may therefore be considered pre-stellar in nature.

The first submillimetre continuum maps of pre-stellar cores were made by Ward-Thompson et al. (1994 – hereafter WSHA). They found that pre-stellar cores are less compact and have larger FWHM sizes than, but comparable masses to, the protostellar envelopes surrounding Class 0 protostars. This is consistent with pre-stellar cores being the precursors of Class 0 protostellar clumps, the latter already having begun to collapse. The WSHA study also suggested that the radial density profiles of pre-stellar cores are relatively steep towards their edges (i.e., sometimes steeper than $\rho(r) \propto r^{-2}$) but flatten out near their centres (becoming less steep than $\rho(r) \propto r^{-2}$). This is apparently inconsistent with the scale-free r^{-2} power-law density distributions characterizing singular isothermal spheres, which are often taken as initial states in protostellar models (see, e.g. Shu et al. 1993, for a review).

The WSHA data did however appear to agree reasonably well with existing theoretical predictions for the radial density profiles of magnetically-supported cores in the ambipolar diffusion phase of low-mass star formation (e.g Mouschovias 1991, Fiedler & Mouschovias 1993). During this phase, the radial core profiles asymptotically approach a $\rho(r) \propto r^{-2}$ power-law (see Lizano & Shu 1989). However, fast dynamical collapse sets in at a relatively early stage, when a substantial region in the center still has a flat density distribution (e.g., Basu & Mouschovias 1995 – hereafter BM95).

Obtaining further observational constraints on the initial conditions for collapse is crucial to get at a better understanding of protostar evolution. In particular, recent theoretical studies show that the mass-infall rate during the protostellar phase is quite sensitive to the initial density profile (e.g. Foster & Chevalier 1993, Henriksen 1994).

In the present paper we discuss new millimetre dust continuum data for one of the pre-stellar cores from the WSHA sample, L1689B. This core corresponds to a $\sim 2' \times 4'$ visually opaque region in the filamentary cloud L1689 of the ρ Ophiuchi molecular complex (adopted distance $d = 160$ pc). The peak position of L1689B was observed in ^{13}CO(1-0), C^{18}O(1-0), and NH_3 by MLB and BM89. The L1689B core is embedded in a large-scale ^{13}CO clump called R65 by Loren (1989a) who mapped it as part of an extensive study of the structure of the ρ Oph complex (see Fig. 1).

The new 1.3 mm data, taken at the IRAM 30-m telescope equipped with the MPIfR bolometer arrays, have $11''$ resolution and were obtained using the on-the-fly mapping technique. They supplement the WSHA 800-μm data, which were taken at JCMT with $18''$ resolution using a point-by-point ('on-off') mapping technique and a single-channel bolometer. As a result, we are now able to rule out any telescope, or technique-dependent, effects which might have affected our previous conclusions on pre-stellar cores. Furthermore, the better sensitivity and spatial sampling of the new data allow us to make a detailed comparison with the predictions of ambipolar diffusion models.

2. Observations and Data Analysis

2.1. Mapping observations

Our 1.3 mm continuum mapping of the pre-stellar core L1689B was carried out with the IRAM-30m telescope located near Granada, Spain, during two observing sessions. The first run on 1995 February 25th and 28th used the 7-channel MPIfR bolometer array, while the second run on 1995 March 18th-19th used the more recent 19-channel MPIfR array. A total of nine 7-channel 'on-the-fly' maps and two 19-channel maps were obtained and co-added. The resulting final map is equivalent to $\sim$ 100 single-channel coverages of a $\sim 3' \times 2'$ (7-channel) or $\sim 4' \times 3'$ (19-channel) effective field of view, with the additional benefit of better sky-noise cancellation and better positional registering of individual coverages. All of the data were taken at night or early morning and most benefited from very good weather conditions. The zenith transmission, monitored by 'skydips' every 1–2 hr, was only $\sim 70\%$ during the first night (Feb. 25th), but reached $\sim 90\%$ the other nights.

The individual on-the-fly coverages were obtained in the dual-beam raster mode with a sampling of $2''$ in azimuth and $4''$ in elevation, a scanning velocity of $4''$/sec in azimuth, and a chopping frequency of 2 Hz. In this observing mode, the telescope is scanned continuously in azimuth along each row while chopping; for each channel, the raw data corresponding to a single on-the-fly coverage

consist of a number of rows (or scans) taken at different elevations. The chop throw was alternately 32″ and 44″ in azimuth in order to improve the restoration process. The passband of the bolometers we used has an equivalent width $\approx$ 70 GHz and is centred at $\nu_{eff} \approx 240$ GHz (e.g., Kreysa 1992; Guélin et al. 1995). At this frequency, the beam size of the telescope was measured to be $\sim 11''$, using Uranus and other strong point-like sources such as quasars. The pointing was checked every $\sim$ 1 hr and found to be accurate to better than $\sim 3''$. Calibration was achieved through on-off observations and on-the-fly mapping of the primary calibrators Uranus and Mars (e.g., Griffin & Orton 1993 and references therein). In addition, the ρ Oph secondary calibrator IRAS 16293-2422, which has a peak 1.3 mm flux $\sim$ 5.3 Jy in an 11″ beam (e.g., André & Montmerle 1994) was observed before and after each L1689B map. Although the relative calibration of individual maps is probably good to within $\sim$ 5–10%, the total, absolute calibration uncertainty is estimated to be $\sim$ 20%. The dual-beam maps were reduced with the new IRAM software for bolometer-array data ("NIC"; cf. Broguière & Neri 1995) which uses the EKH restoration algorithm (Emerson, Klein, & Haslam 1979). The final unsmoothed map (not shown here), which results from the combination of all 11 multi-channel coverages, has an estimated rms noise of $\sim$ 5 mJy per 11″ beam in its central $\sim 3' \times 1.5'$ (observed by all channels).

Figure 2 shows the final co-added 1.3-mm isophotal contour map of L1689B superposed on a grey-scale image, after it has been smoothed to 13″ angular resolution for better sensitivity. The rms is now $\sim$ 3 mJy per 13″ beam. In this map, the main component of the L1689B core is clearly resolved and appears as an east-west elongated source of aspect ratio $\sim$ 0.7. In addition, a secondary, fainter component is visible $\sim 80''$ to the north-west of the main core. Its presence probably explains the apparent SE-NW elliptical shape seen in the 800μm map of WSHA taken at lower angular resolution (18″). The characteristics of these sources, estimated from two-dimensional Gaussian fits to the smoothed map of Fig. 2, are given in Table 1 which lists positions, peak fluxes, deconvolved sizes, and position angles. The parameters of the secondary component are particularly uncertain because of its faint and diffuse appearance. Note that the results of our single-component Gaussian fit (last line of Table 1) are in very good agreement with the properties derived by WSHA. Finally, we stress that the actual structure of L1689B is probably more complicated than a simple elliptical Gaussian source. In particular, the core seems to be pinched in the north-south direction (see end of Sect. 2.2 below).

2.2. Flux Density Profiles and Morphology

To further investigate the structure of the L1689B core, we made various estimates of the radial flux density pro-

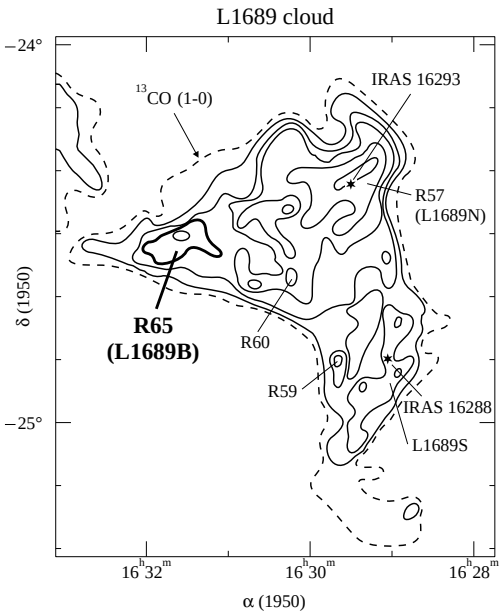

Fig. 1. Large-scale spatial distribution of the (low-density) molecular gas in the L1689 cloud (adapted from Fig. 3c of Loren 1989a). The contours represent the ^{13}CO(1–0) line intensity measured at $V_{LSR} = 3.83$ km s^{-1} by the MWO 4.9 m telescope (2.4′ beam) and go from $T_R^* = 2$ K (dashed line) to $T_R^* = 12$ K by steps of 2 K. The L1689B core studied in this paper is embedded within the clump denoted R65 by Loren.

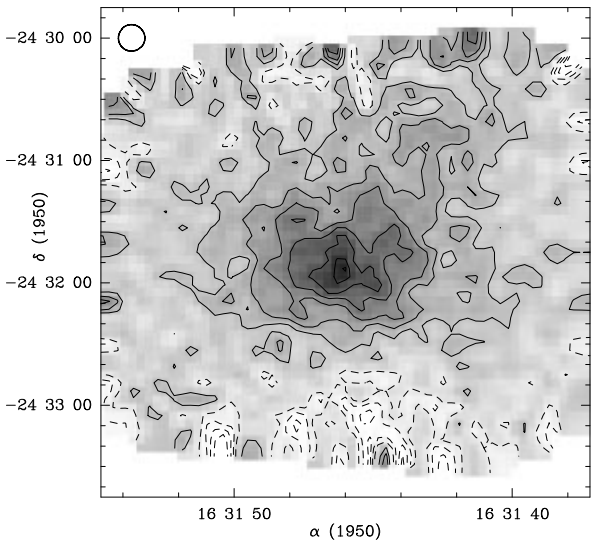

Fig. 2. "On-the-fly" 1.3mm continuum map of the prestellar core L1689B obtained with the MPIfR 7-channel/19-channel arrays in Feb./March 1995. This map results from the combination of 11 multi-channel coverages and was smoothed to an effective angular resolution of 13″. Contour levels go from −40 to −10 mJy/beam (dotted lines) and from 10 to 60 mJy/beam (solid lines) with steps of 10 mJy/beam. The rms noise level is $\sim$ 3 mJy/13″ beam. The effective FWHM beam size is shown in the upper left corner.

Table 1. Results of Gaussian fits to the 13″-resolution map

Source	R.A.(1950)	Dec.(1950)	S_g^{peak} (mJy/beam)	FWHM (″)	P.A.[a] (deg)
Main component	$16^h31^m46\overset{s}{.}1$	$-24°\ 31'\ 54''$	51 ± 3	86×58	90 ± 20
2nd component	$16^h31^m43\overset{s}{.}0$	$-24°\ 30'\ 45''$	20 ± 10	$\sim 130 \times 70$	100 ± 50
Global	$16^h31^m45\overset{s}{.}9$	$-24°\ 31'\ 43''$	48 ± 3	94×66	105 ± 5

[a] The position angle of the major axis is measured from north to east.

file through the main component of Fig. 2 and Table 1. Our first, simple approach was to assume the source to be circularly symmetric in the plane of the sky and to average the signal in circular annuli centered on the peak position. In order to avoid confusion from the secondary component, the data present in the north-west quadrant were ignored in this averaging. Figures 3a and 3b show the resulting azimuthally-averaged profiles, obtained from the unsmoothed 11″-resolution map, in linear-linear format and log-log format respectively. The error bars are $\pm 1\sigma(\theta)$, where the rms noise $\sigma(\theta)$ was estimated on the map in a region with no or little signal and scaled to each annulus of angular radius θ according to the number of dual-beam data points constraining the emission in that annulus.

In a second step, we tried to take the asymmetry of the core into account. Figure 3c shows radial flux profiles along the major and minor axes of the main source, obtained by averaging the emission in the 13″-resolution map over a 40° east-west sector and a 40° north-south sector, respectively. (The smoothed data were used in this case to improve the signal-to-noise.) While the east-west profile is roughly consistent with the azimuthally-averaged profile of Fig. 2b, the north-south profile appears to be significantly steeper.

We also averaged the emission over elliptical rings of axis ratio 0.7 rather than over circular annuli as in Figs. 3a and 3b. The corresponding radial intensity profile, shown in Fig. 3d, would more reliably describe the intrinsic source profile than that of Fig. 3b if the true three-dimensional geometry of the core were a disk inclined to the line of sight. We stress here that the sampling of the radial profiles shown in Fig. 3 is five times better than the sampling of Figs. 3 and 4*c* of WSHA. This, coupled with the higher angular resolution, allows us to set stronger constraints on theoretical models (see Sect. 3 below).

The circularly-averaged and elliptically-averaged profiles of L1689B (Fig. 3b and Fig. 3d) appear to have a break at $\theta \sim 25''$. However, the observing technique (dual-beam mapping) and reduction method (baseline subtraction and restoration) may affect the shape of the radial profiles of Fig. 3. In order to quantify these effects and accurately compare our observational results with simple models, we thus performed a number of simulations (see, e.g., Motte, André, & Neri 1995). Starting with several model sources, such as power laws of the form $I(\theta) \propto \theta^{-m}$ or Gaussians, we first generated synthetic dual-beam maps simulating those that would be observed by the various channels of the bolometer array in the on-the-fly scanning mode (including a convolution with the beam of the telescope). We then reduced the simulated dual-beam maps in exactly the same way as the real data, and derived the associated radial flux profiles. Some of these simulated profiles are displayed in Figure 3. The profile shown as a dash-dotted line in Fig. 3b corresponds to the simulated observation of an axisymmetric model source with $I(\theta) \propto \theta^{-1}$ at all angular radii down to an inner radius $\theta_{in} = 1''$ (which is much smaller than the beam size). The dotted line corresponds to a model source with $I(\theta) \propto \theta^{-0.3}$ up to an angular radius $\theta = 25''$ and $I(\theta) \propto \theta^{-1}$ for $\theta > 25''$. The dash-dotted line in Fig. 3d and the dotted lines in Figs. 3c and 3d show simulated profiles corresponding to elliptical models of aspect ratio 0.7 which have the same angular dependence along their major axis as the models of Fig. 3b. The observed profiles are not consistent with the single power-law models (dash-dotted lines) and the discrepancy would be stronger if a smaller value of θ_{in} had been adopted. The two-component models (dotted lines) describe the data much better.

Comparison between the observed and simulated profiles shows that the break in the slope of the observed profile is real and occurs at $\theta = 25'' \pm 5''$. It is also clear that a small fraction of the signal is lost at large angular radii, making the profiles look steeper than the source and the models actually are. The "best-fit" slope we derive for the flat inner region ($0'' < \theta < 25''$) is $m = 0.3 \pm 0.2$ assuming an axisymmetric source (Fig. 3b), and $m = 0.2 \pm 0.2$ assuming an elliptical source (Fig 3d). In the outer region ($25'' \lesssim \theta \lesssim 90''$), the averaged profile is roughly consistent with models having $m \simeq 1.0 \pm 0.3$, independently of the symmetry assumed. (Note, however, that the circularly-averaged profile of Fig. 3b is somewhat steeper than $m = 1$ beyond $\theta \sim 70''$.)

The circularly-averaged (Fig. 3b) and elliptically--averaged (Fig. 3d) profiles of L1689B are *not* consistent with simple Gaussian models, such as those used in some numerical simulations of protostellar collapse (e.g. Boss 1987). These models produce too sharp an outer edge. The data would be better represented by a two-component

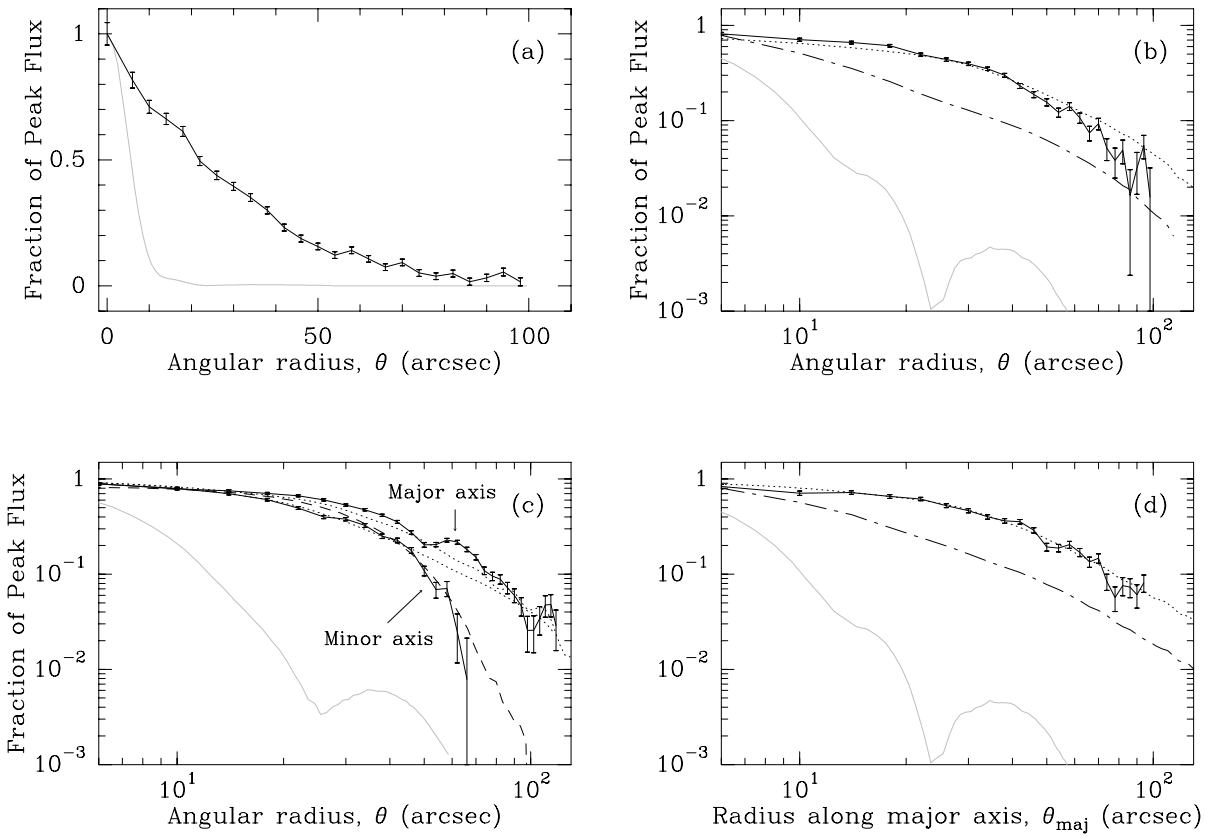

Fig. 3. Normalized radial flux-density profiles of the L1689B core (solid lines) obtained by averaging the observed 1.3 mm emission under circular [(a), (b)] or elliptical [(c), (d)] symmetry assumptions. In all panels, the beam profile is shown as a light dotted line for comparison.
(a) Azimuthally-averaged profile in linear-linear format.
(b) Azimuthally-averaged profile in log-log format compared to the simulated profiles of two model sources. The dash-dotted line corresponds to a model of the form $I(\theta) \propto \theta^{-1}$ down to $\theta = 1''$. The dotted line represents a model such that $I(\theta) \propto \theta^{-0.3}$ for $\theta \leq 25''$ and $I(\theta) \propto \theta^{-1}$ for $\theta \geq 25''$.
(c) Log-log intensity profiles along the major (upper solid curve) and minor (lower solid curve) axes of the core, obtained by azimuthally averaging the signal observed in the smoothed map of Fig. 2 over 40° sectors. These observed profiles are compared with the similarly averaged major and minor profiles of an elliptical model of aspect ratio 0.7 such that $I(\theta_{maj}) \propto \theta_{maj}^{-0.3}$ for $\theta_{maj} \leq 25''$ and $I(\theta_{maj}) \propto \theta_{maj}^{-1}$ for $\theta_{maj} \geq 25''$ (dotted lines). The dashed line shows the simulated profile of a $57''$ (FWHM) Gaussian model which fits most of the minor axis profile of L1689B.
(d) Elliptically-averaged intensity profile in log-log format, compared with simulated profiles (dotted and dashed-dotted lines) corresponding to elliptical models with the same angular dependence along their major axis as the models shown in (b). A position angle of 90° and an aspect ratio of 0.7 were assumed for the elliptical averaging.

Gaussian model: an unresolved point source of 10 mJy per $11''$ beam and a $90'' \times 63''$ elliptical Gaussian of peak flux 40 mJy/beam. However, even such a two-component model produces too little emission at large angular radii ($\theta > 70''$) and does not fit the observations as well as the second power-law model described above. The presence of a central point source could potentially reflect the fact that the core has already formed a protostar. However, the weakness of the central peak and the broad intensity plateau characterizing the extended component would be in marked contrast with the radial intensity profiles of known protostars (e.g. Ladd et al. 1991, AWB93, Motte et al. 1995). We therefore favor the prestellar interpretation of WSHA and tentatively attribute the peak to a local inhomogeneity which may trace the onset of a Jeans-like instability (see Sect. 3).

The radial intensity profile measured along the core minor axis is very steep in its outer part (see Fig. 3c). In contrast to the major axis profile, the north-south profile of L1689B is steeper than the $I(\theta) \propto \theta^{-1}$ model for

$\theta \gtrsim 45''$ (dotted lines in Fig. 3c), and would in fact be better described by a Gaussian model (dashed line in Fig. 3c). The circularly-averaged profile (Fig. 3b), which includes a significant contribution from the minor axis, is itself steeper than the power-law models for $\theta \gtrsim 70''$. We suggest that we may be seeing the edge of the cloud core in the north-south direction. In agreement with this view, the isophotal contours of Fig. 2 are "pinched" in the north-south direction and the map exhibits negative levels in its northern and southern parts. These negative levels are not just random noise since they appear consistently in each mapping coverage. Since the parallactic angle was close to 0° in all the coverages, the negative "emission" occurs roughly perpendicular to the scanning direction and cannot result from the above-mentioned loss of signal at large angular radii (which is more severe along the chopping direction – azimuth). We believe the negative levels at the top and bottom of Fig. 2 are an artefact of the reduction technique and may be understood as follows. The restoration process assumes that there is no emission at the ends of each map row (Emerson et al. 1979). If the source size is actually comparable to (or larger than) the map size, then this assumption is invalid. Furthermore it can be seen in Fig. 2 that the source has a shape resembling an "hourglass" oriented east-west, i.e., approximately in the scanning direction. Therefore, along the upper and lower rows of a dual-beam map, the emission at the scan edges will be stronger than at the scan centre. Hence, when the restoring algorithm sets the scan edges to zero, it creates apparently negative signal at the scan centre. Although this reconstruction problem is easy to verify on dual-beam simulations of an hourglass-shaped model source, it is more difficult to assess the true importance of the effect with no further assumption about the actual core geometry. Since no negative levels are present in the inner $2' \times 2'$ of the map, the problem is not significant on small spatial scales, and the inner $60''$ parts of the profiles, at least, can reliably be trusted.

2.3. Mass Distribution

Since millimeter continuum emission is optically thin, it is a direct tracer of the mass content of protostellar cores. For a spherical isothermal dust source, the total (dust + gas) mass, $M(R)$, contained within a radius R of the center, is related to the millimeter flux density $S_{1.3mm}(\theta)$ integrated over a circle of projected angular radius $\theta = R/d$ by the equation:

$$M(R) = [S_{1.3mm}(\theta)\, d^2]/[\kappa_{1.3}\, B_{1.3}(T_{dust})],$$

where $\kappa_{1.3}$ is the dust opacity per unit mass column density at $\lambda = 1.3$ mm and $B_{1.3}(T_{dust})$ is the Planck function at $\lambda = 1.3$ mm, for a dust temperature T_{dust}.

The dust temperature derived by WSHA was 15^{+3}_{-7} K, based on the spectral energy distribution (SED) of the flux densities of L1689B measured at JCMT, combined with the IRAS upper limits corresponding to the non-detection of this source in the far-infrared. The temperature thus derived is clearly quite uncertain, since the spectrum peaks precisely in the far-infrared (see Fig. 5 of WSHA), and it is the peak of the SED which determines the temperature. The kinetic gas temperature, T_K, was found to be ~ 20 K by both MLB and Loren (1989a), based on observations of ^{13}CO and C^{18}O respectively.

Since the CO observations were taken at lower angular resolution than the dust continuum observations, it is possible that the gas kinetic temperature of 20 K merely represents the temperature of the large-scale cloud R65 (Loren 1989a), while the embedded dense core we observe in the continuum is colder, with a temperature of only ~ 15 K (or less). Since starless cores/clouds are presumably heated from the outside, their dense inner regions may indeed be expected to be colder (see, e.g., Falgarone & Puget 1985). Recent high-resolution C^{18}O observations of L1689B (Ward-Thompson & Jessop 1996) tend to support this view. However, given the uncertainties described above, we cannot say for sure that we are observing this effect. Thus, in the following, we take the mean of the three derived temperatures, and use a uniform core temperature of $T = 18$ K.

The mass opacity $\kappa_{1.3}$, which depends on the dust-to-gas ratio, as well as the composition, shape, and size distribution of the dust grains, is also somewhat uncertain (see Henning, Michel, & Stognienko 1995, for a recent review). In this paper, we adopt the dust opacity recommended by Henning et al. (1995) and Preibisch et al. (1993) for clouds of intermediate densities ($n_{H_2} \lesssim 10^5\ cm^{-3}$), and we assume a standard gas to dust mass ratio of 100, yielding $\kappa_{1.3} = 0.005$ cm^2 g^{-1}. Based on the discussion of Henning et al. (1995) and Krügel & Siebenmorgen (1994), we estimate that our adopted value of $\kappa_{1.3}$ should apply to the core of L1689B to within a factor of $\sim$ 2–3 uncertainty.

With these assumptions, we can estimate the mass of L1689B within various angular radii from its center. Since we observe the core to be elliptical with axis ratio of 0.7, we measure the flux density, and hence the mass, within elliptical regions of axis ratio 0.7. Figure 4 shows a plot of the mass $M(\theta_{maj})$ contained within such elliptical regions as a function of the ellipse semi-major axis θ_{maj}. The solid line in Fig. 4 represents mass estimates derived from direct flux integration in the map of Fig. 2, without any correction for the loss of flux density occurring at large angular radii (see Sect. 2.2 above). The dotted line shows a curve of the form $M(\theta) \propto \theta^2$ which fits the observations at small angular radii, i.e., within the flat inner region. The dashed line shows the linear relation $M(\theta) \propto \theta$ which best approximates the data in the outer region. Comparison of the dashed and solid lines of Fig. 4 suggests that we start to loose significant flux (hence significant mass) at angular radii larger than $\theta_{maj} \sim 50''$ due to the finite size of the map. For this reason, it is best to use the dashed line to estimate the mass contained within large radii.

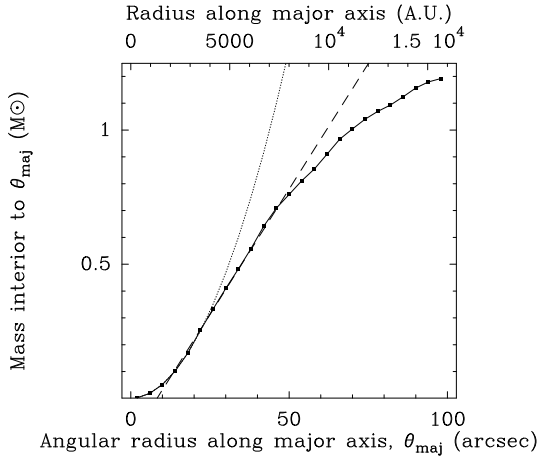

Fig. 4. Mass contained within ellipses of aspect ratio 0.7 and major radius θ_{maj} as a function of θ_{maj}. The mass was estimated from the flux mapped at 1.3 mm with 11″ resolution assuming $T = 18$ K and $\kappa_{1.3} = 0.005$ cm^2 g^{-1} (see text). The dotted and dashed lines show the relations $M \propto \theta_{maj}^2$ and $M \propto \theta_{maj}$ which best approach the observations for $\theta_{maj} < 25''$ and $\theta_{maj} > 25''$, respectively. The dashed, staight line represents our best estimate of the outer mass profile after correction for the loss of flux occurring at large angular radii.

The central plateau region of angular radius $\sim 25''$ (corresponding to $\sim$ 4000 AU) is of particular interest since this is the radius at which the flux density profiles of Fig. 3b and Fig. 3d show a break, becoming steeper outside of this radius. This inner plateau region has a mass $M_{flat} \sim 0.33\ M_\odot$. Assuming this inner plateau region is approximately spherical, its average number density is $n_{H_2}^{flat} \sim 2 \times 10^5\ cm^{-3}$. In addition, based on Fig. 4, we estimate masses of $\sim 0.4\ M_\odot$, $\sim 1\ M_\odot$, and $\sim 2.1\ M_\odot$ within angular radii of 30″, 60″, and 120″ from core center respectively (corresponding to physical radii of 4800 AU, 9600 AU, and 19000 AU). Note that the mass M(120″) is more uncertain than the others due to the abovementioned loss of flux density at large angular radii.

The mass derived by WSHA within a 30″ radius of L1689B was 1.2 $M_\odot$, assuming a temperature of 15 K (see their Table 2). If we recalculate this using a temperature of 18 K we obtain a mass, based on the 800-μm continuum data, of $\sim$0.9 $M_\odot$. This lies between the values derived here for 30″ and 60″ radii based on the 1.3-mm data. We believe that the difference between the masses derived from the two datasets arises from the lower resolution and sampling rate of the 800-μm data. This caused the peak observed at 800 μm to be shifted slightly to the north-west, due to the presence of the second component to the north-west discussed in Sect. 2.1 above. Hence the mass derived in a 30″ radius from the 800-μm data includes more of the north-west component than the 30″ radius mass derived from the 1.3-mm data in this paper, and is closer to the value derived for the 1.3-mm, 60″ radius mass. We believe therefore that the current mass estimates more accurately reflect the true mass of the main component of L1689B.

3. Discussion

3.1. Boundary conditions: the parent cloud R65

The large-scale ^{13}CO clump R65 (see Fig. 1) in which L1689B is embedded has an estimated mass $M \approx 39\ M_\odot$, temperature $T \approx 20$ K, FWHM size $\approx 0.77 \times 0.44$ pc, mean density $n_{H_2} \approx 6.5 \times 10^3$ cm^{-3}, and one-dimensional velocity dispersion $\sigma_{tot} \approx 0.39$ km s^{-1} (Loren 1989a). This clump or "cloud" harbors no known embedded YSO but appears to be gravitationally bound and in the process of forming one or more stars. Indeed, although R65 appears to have a slight excess of kinetic (turbulent) energy, it is very close to gravitational virial equilibrium with an estimated $M/M_{vir} \approx 0.7$. This contrasts with the majority of the clumps studied by Loren (1989b) which are much farther from gravitational virial equilibrium and typically have $M/M_{vir} \lesssim 0.1$. Even these non-selfgravitating clumps are not believed to be transient structures but rather clumps confined by external pressure (Bertoldi & McKee 1992; Blitz 1993). While pressure-confined clouds are expected to have approximately uniform densities (Bertoldi & McKee 1992), R65 is centrally condensed, as indicated by the NH_3 detection of BM89 and the peaked dust continuum profile found in WSHA and the present study. This indicates that self-gravity has been playing a major role in the recent evolution of R65. In particular, we stress the density peak corresponding to L1689B is about an order of magnitude stronger than the small, unbound density fluctuations generated by turbulence in quiescent molecular clouds (see Falgarone, Puget, & Pérault 1992).

In fact, if thermal pressure were the only means of support against gravity, R65 would be gravitationally unstable since its mass is much larger than the critical Bonnor-Ebert mass (e.g., Bonnor 1956) $M_{BE} = 2.4\,Ra^2/G \approx 11\,M_\odot$ (where a is the isothermal sound speed corresponding to $T = 20$ K). We also note that the density contrast between the peak of L1689B and the edge of R65 is $\gtrsim 30$, i.e., significantly larger than the maximum contrast of ~ 14 for a stable self-gravitating isothermal sphere (Bonnor 1956). Assuming R65 is in quasi-equilibrium, it must therefore be supported against collapse by magnetic fields, turbulence, or a combination of both.

3.2. Comparison with models of core structure

Since dust emission is optically thin at 1.3 mm, the radial flux profiles shown in Fig. 3 should directly reflect the intrinsic column density profile of the L1689B core, provided the dust temperature T_{dust} and absorption coefficient $\kappa_{1.3}$ remain roughly constant through the source. In the outer

parts of the core where the density is lower, T_{dust} may increase somewhat (see Falgarone & Puget 1985), while $\kappa_{1.3}$ may decrease (e.g. Krügel & Siebenmorgen 1994) and approach the value appropriate to the diffuse interstellar medium (i.e., ~ 0.002 cm^2 g^{-1} instead of our adopted 0.005 cm^2 g^{-1}; see Draine & Lee 1984). We neglect these two potential effects which tend to cancel out and should not affect the dense central region.

The intensity profile we observe therefore indicates that L1689B has a relatively flat column-density profile in its inner region. The structure of this core is thus not adequately described by a singular isothermal sphere model (e.g. Shu et al. 1987) or by a singular sphere model with thermal and nonthermal motions ("TNT" model; Myers & Fuller 1992). On the other hand, it is qualitatively consistent with equilibrium models for thermally-supported, self-gravitating condensations of mixtures of gas and dust (e.g., Bonnor 1956; Falgarone & Puget 1985; Chièze & Pineau des Forêts 1987), and with magnetically-supported core models at various stages of the ambipolar diffusion phase (e.g. Mouschovias 1991, Lizano & Shu 1989). The first class of models ignore the role of magnetic fields, but do not assume an isothermal equation of state; they generalize the isothermal Bonnor-Ebert sphere by taking into account the heating influence of the interstellar UV radiation field. The second class of models include magnetic fields but are generally isothermal. We note here that a non-magnetic model intermediate between models #2 and #3 of Falgarone & Puget (1985), which have central densities $n_0 = 10^5\ cm^{-3}$ and $n_0 = 10^6\ cm^{-3}$ respectively, would approach the observed density structure of L1689B quite well. However, these models predict a strong increase in temperature (with $T \gtrsim 30$ K) at radii larger than ~ 0.1 pc, which is only marginally consistent with the ^{13}CO observations of Loren (1989a). Since the magnetic models are far more comprehensive (i.e., they account not only for the density structure but also for the formation and evolution of cores), we will focus the remainder of the discussion on a detailed comparison between their predictions and our observations.

3.2.1. Predictions of the magnetic core models

If molecular clouds are primarily magnetically-supported, then gravitationally-driven ambipolar diffusion can explain the progressive formation and self-initiated collapse of dense cores (e.g., Mouschovias 1991; Shu, Adams & Lizano 1987). In recent years, Mouschovias and collaborators have carried out an extensive numerical study of the evolution of isothermal, axisymmetric model clouds threaded initially by a uniform magnetic field (see Mouschovias 1995 and references therein).

The model clouds are assumed to be thermally supercritical (i.e., self-gravitating), but initially magnetically subcritical. During the quasi-static ambipolar diffusion phase, a force balance between thermal pressure and gravity is established relatively rapidly along the field direction, while lateral contraction proceeds only as rapidly as magnetic forces allow. The relevant evolutionary timescale is the ambipolar diffusion timescale, which is $t_{AD} = 2 \times 10^6\,(x/10^{-7})$ yr for a typical value of the ionization fraction x in the initial cloud (see Nakano 1979). During this phase, the central mass-to-flux ratio, $(M/\Phi)^{cent}$, increases until it reaches the critical value (e.g., Mouschovias 1991):

$(M/\Phi)^{cent}_{crit} = 1.5\,(63G)^{-1/2}$.

This corresponds to the formation of a both magnetically and gravitationally supercritical core, while the bulk of the cloud (the 'envelope') remains magnetically supported.

The supercritical core then collapses in a dynamical but magnetically-controlled fashion, while the surrounding envelope of the cloud remains magnetically supported. At all stages, except perhaps the very early ones, the model clouds are disk-like, with minor axes lying parallel to the magnetic field direction, and are characterized by a relatively flat-density, central region, of polar radius (e.g. Mouschovias 1991, Fiedler & Mouschovias 1993):

$Z_{T,cr} \approx a\,(2\pi G\rho_c)^{-1/2}$,

which is determined by the balance of gravitational and thermal-pressure forces along field lines. In this expression, a is the isothermal sound speed and ρ_c is the central density. Likewise, prior to the formation of the supercritical core, the equatorial extent of the central region is fixed by magnetic support and it scales as the critical magnetic length:

$\lambda_{M,cr} \propto B/\rho$.

After a supercritical core has formed, the central, flat-density region is nearly spherical and has an equatorial radius determined by the critical thermal length scale:

$\lambda_{T,cr} = \frac{\pi}{2}\,Z_{T,cr}$.

Outside the central region, the density declines sharply, with a variable power-law index $s = -dln\rho/dlnr$, typically in the range $s = 1.5$–3, depending on radius and the exact initial conditions (e.g., BM95).

The evolution of the supercritical core leads to the formation of a protostar in a relatively short time $\sim 10^6$ yr (see, e.g., Fig. 2d of Ciolek & Mouschovias 1994). Typically, the time taken by a molecular cloud core to become magnetically supercritical is $\sim 10^7$ yr, i.e., $\sim$10 times as long as the subsequent time for the supercritical core to collapse and form a hydrostatic protostar, depending on the initial conditions (BM95). Once formed, such a protostar should be observable as a Class 0 (or subsequently a Class I) source in the radio (and subsequently infrared) wavelength range.

3.2.2. Observational constraints

Since there is no evidence for any infrared or radio continuum source at the center of L1689B (Beichman et al. 1986; Bontemps 1996), it is likely that this core has not yet formed a hydrostatic protostar. Assuming L1689B does

not differ in its properties from the other cores detected by WSHA in the submm continuum, its evolution should occur on a timescale of order $\sim 10^6$ yr (cf. WSHA). Given this lifetime and the central density estimated in Sect. 2.3 ($n_{H_2}^{flat} \sim 2 \times 10^5\ cm^{-3}$), comparison with the models of BM95 and Ciolek & Mouschovias (1994; in particular, see their Fig. 2d) suggests that L1689B is either near the end of the quasi-static phase or close to the beginning of the dynamical phase of contraction (if it can be explained by the magnetic support model at all).

The inner, relatively flat density region we observe in L1689B (see Sect. 2.2 above) has a radius $R_{flat} \sim$ 4000 AU and a mass $M_{flat} \sim 0.33$ M$_\odot$, hence a surface density:

$\Sigma_{flat} \approx M_{flat}/(\pi R_{flat}^2) \sim 0.05\ g\,cm^{-2}$.

In the particular axisymmetric geometry of the magnetically-supported core models, the Jeans criterion for gravitational instability can be written as (e.g., Ciolek 1996):

$M_{flat} \geq M_{Jeans}$, with $M_{Jeans} = \frac{\pi}{2} R_{flat} a^2/G$.

Since our estimated value of M_{flat} scales approximately as T^{-1} (Rayleigh-Jeans regime), we have: $M_{flat}/M_{Jeans} \approx 0.75 \times (T/18K)^{-2}$. The central temperature of L1689B is relatively uncertain and may well be lower than 18 K (see Sect. 2.3) for pre-stellar cores are generally predicted to be colder in their central regions (e.g. Falgarone & Puget 1985, Lizano & Shu 1987), . We conclude that our present data are consistent with the central flat region of L1689B being self-gravitating.

It is easy to estimate the mean magnetic field strength required to support this dense core against collapse. Since the magnetic strength is related to the magnetic flux by:

$B_{flat} = \Phi_{flat}/(\pi R_{flat}^2)$,

L1689B will be magnetically subcritical if:

$M_{flat}/\Phi_{flat} = \Sigma_{flat}/B_{flat} < (M/\Phi)_{crit}^{cent}$,

which may also be written as:

$B_{flat} > B_{crit} = \Sigma_{flat}/(M/\Phi)_{crit}^{cent} \approx 80\ \mu$G.

This is somewhat higher than typical initial cloud values quoted in the literature. However, Goodman & Heiles (1994) measured the line-of-sight magnetic field strength $B_{||}$, using Zeeman measurements of HI, towards more than 50 positions in the Ophiuchus region, and found the highest value of $B_{||}$ ($\sim 20\mu$G) towards their position #34 which encompasses R65 (and L1689B). The ~ 0.7 aspect ratio we observe is consistent with the disk-like geometry of the magnetic models and may be interpreted as resulting from a disk inclination angle $i \sim 45°$. Using this estimated inclination angle, the total field strength would be 40% larger than $B_{||}$. The HI measurements made with a very large beam ($36'$) sample the large-scale magnetic field in a component of low-density ($n < 100$ cm^{-3}) atomic gas along the line of sight, which may or may not be related to the field in the denser ($< n(H_2) > \sim 7 \times 10^3$ cm^{-3}) molecular gas of R65/L1689B. The smaller-scale field in the molecular gas may easily be a factor of 2 or more larger than the large-scale field. Furthermore, the optical polarization measurements of Vrba, Strom, & Strom (1976) show a large dispersion of polarization directions in L1689 compared to other clouds without clusters, which suggests that, on a large-scale at least, the non-uniform component of the magnetic field is far from negligible in this region (see Myers & Goodman 1991). Assuming that the non-thermal component $\sigma_{NT} = 0.24$ km s^{-1} of the velocity dispersion measured by Loren (1989b) at the position of R65 in a $2.4'$ beam correspond to magnetic motions of both wavelike and turbulent character whose kinetic energy density equals the magnetic energy density, one has $\sigma_{NT}^2 = V_A^2/3$, where $V_A = B/(4\pi\rho)^{1/2}$ is the Alfvén velocity (Myers & Goodman 1988). Using our present density estimates, this assumption would imply a mean magnetic field $B \sim 60\ \mu$G within a radius ~ 11500 AU, which is close to our above upper limit for B_{flat}. For all these reasons, we do not believe that a value $\lesssim 80\,\mu$G for the mean magnetic field at the center of L1689B is unfeasible. We also note that the magnetic model itself predicts a typical increase of the central field strength by a factor $\lesssim 2$ over its initial value during the quasi-static phase of cloud contraction (e.g., Mouschovias 1991). After the formation of a supercritical core, the central magnetic field of the models increases with density roughly as $B \propto n^{0.5}$, and the condition $B > B_{crit}$ is no longer satisfied.

In the framework of the ambipolar diffusion models, therefore, our above estimates of M_{Jeans} and B_{crit} indicate that L1689B is either magnetically critical or only slightly subcritical. This is because the actual magnetic field is unlikely to be much stronger than 80 μG and because the estimated mass of the central region is consistent with M_{Jeans}. We conclude that the central region of L1689B either has just entered the dynamical phase of protostellar collapse or will soon do so.

If L1689B is indeed close to critical, the radius R_{crit} of the (either existing or forthcoming) supercritical core should be of the same order as R_{flat}, i.e., $R_{crit} \sim 0.02$ pc.

An upper limit to the final mass of the protostar that L1689B will form is given by the sum of the mass M_{flat} of the present flat inner region and the mass M_{fed} which will be fed into the supercritical core. M_{fed} depends on how well the cloud envelope is magnetically supported, which in turn depends on the exact degree of ionization (see Ciolek & Mouschovias 1995). A reasonable estimate (Ciolek 1996) is that $M_{flat} + M_{fed}$ is comparable to the central Jeans mass $M_{T,cr}(t_0)$ of the parent cloud at the onset (t_0) of significant ambipolar diffusion. Since the Jeans mass scales as $M_{T,cr} \propto n^{-1/2}$ with density, we estimate $M_{T,cr}(t_0) \sim 2\ M_\odot$ assuming the initial central density was close to the mean density observed in R65 (cf. Sect. 3.1). Thus we predict that L1689B will form a protostar of mass ~ 0.3–$2\ M_\odot$.

3.2.3. The radial density profile of L1689B

We may go further and make more detailed comparisons between our results and theoretical predictions for the density structure of pre-stellar cores.

The radial density profile of L1689B (see Fig. 5) may be derived from the observed intensity profiles (Fig. 3), assuming that we know the cloud geometry.

First, we assume spherical symmetry. If $\rho(r) \propto r^{-p}$, $T(r) \propto r^{-q}$ are the density and temperature distributions as a function of radius r, and $I(\theta) \propto \theta^{-m}$ is the observed intensity profile as a function of projected radius θ, then at large θ p, q and m are related by the simple equation $p = m - q + 1$ when $p + q > 1$ (e.g., Adams 1991). For an isothermal source $q = 0$, and the equation simplifies to $p = m + 1$ (valid for $p > 1$). Using the estimates of m obtained in Sect. 2.2, we conclude that if L1689B is roughly ellipsoidal in shape then its density gradient must be $1.0 \lesssim p \lesssim 1.4$ at radii $r \lesssim R_{flat}$ and $p \approx 2$ at radii $r \gtrsim R_{flat}$. Figure 5 displays this density profile as a dashed line.

However, if L1689B is indeed a magnetically-supported core, it should be flattened along the direction of the mean magnetic field. We therefore make a second estimate of the density gradient assuming L1689B can be described by the same thin disk geometry as the numerical models of Mouschovias and collaborators (see, e.g., Fig. 1 of BM95). In these axisymmetric models, the column density perpendicular to the equatorial plane scales as $\sigma(r) \propto \rho(r)\, Z_{T,cr} \propto \rho^{1/2}(r)$ (see the expression given in Sect. 3.2.1 above for $Z_{T,cr}$). The core density profile as a function of equatorial radius r_{eq} may thus be derived from the elliptically-averaged intensity profile $I(r_{eq})$ (see Fig. 3d) as $\rho(r_{eq}) \propto I^2(r_{eq})$. Therefore, one has $p = 2m$ in this disk geometry. The density gradient is again inferred to be $p \approx 2$ in the outer region, but this time $0 \lesssim p \lesssim 0.8$ in the flat inner region, which is in better agreement with the predictions of the magnetic models. This density profile is displayed in Fig. 5 as a solid line.

We note that the core density cannot continue to decrease as $\rho(r) \propto r^{-2}$ much beyond the region we have mapped. Indeed, this would imply a density contrast between the center of L1689B and the edge of R65 of ~ 200, much larger than the observed value of ~ 30. At large radii, nonthermal turbulent support is likely to dominate over thermal support, yielding a shallower density gradient $\rho(r) \propto r^{-1}$ (e.g., Myers & Fuller 1992; see also Fig. 10 of Falgarone & Puget 1986). Assuming the nonthermal velocity dispersion σ_{NT} increases with radius as $r^{0.5}$ within R65, the observations of Loren (1989b) indicate that the thermal and nonthermal velocity dispersions are equal at a radius $r_{TNT} \sim 1.6 \times 10^4$ AU from the peak of L1689B. If nonthermal motions exert an isotropic kinetic pressure $\rho\,\sigma_{TNT}^2$, then the density gradient is expected to approach $\rho(r) \propto r^{-1}$ beyond a radius $r_0 \approx 3\, r_{TNT} \sim 4.7 \times 10^4$ AU (see Myers & Fuller 1992). With these parameters, the density averaged over the radius $R_{mean} \approx 0.29$ pc of the parent cloud R65 would be $< n(H_2) > \approx 3.5 \times 10^3$ cm^{-3}, which is only a factor of 2 lower than the density estimated by Loren (1989a).

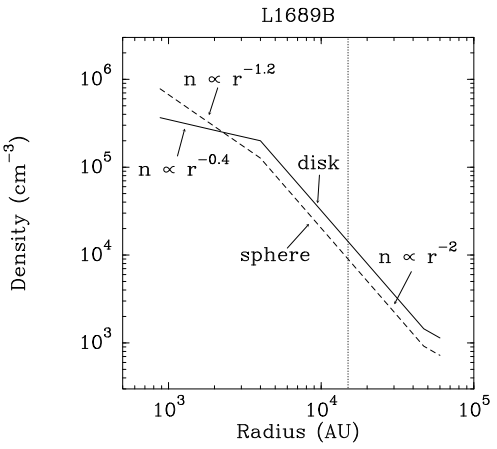

Fig. 5. Average radial density profile of L1689B derived from our observations under two de-projection hypotheses. The solid line assumes the core has the same disk-like shape as the magnetic models of Mouschovias and coworkers (see text). The dashed line assumes ellipsoidal geometry. Our data constrain the density structure of L1689B only at radii $r \lesssim 15000$ AU, i.e., to the left of the vertical dotted line. The profiles have been extrapolated to larger radii assuming the nonthermal model of Myers & Fuller (1992) applies there (see text).

3.2.4. Nature of the north-south "edge"

As noted in Sect. 2.2, the radial intensity profile of L1689B becomes very steep in the north-south direction beyond a radius $r \sim 10^4$ AU. This is suggestive of a sharp edge in that direction. If real, this edge may have several interpretations.

The non-isothermal but thermally-supported core models of Falgarone & Puget (1985) feature a core–halo structure, in which an isothermal core is separated from the cloud 'envelope' by a layer with a steep density gradient (s up to ~ 4) and a low kinetic temperature. In these spherical models, the steepest density gradient typically occurs in the range $r \sim 1.4$–2.5×10^4 AU (see Table 2 of Falgarone & Puget 1985; see also Fig. 10 of Falgarone & Puget 1986), which is roughly consistent with our observed profile of L1689B in the north-south direction. However, these non-magnetic, non-rotating models provide no obvious explanation for the asymmetry of the core.

The magnetically-supported core models of Mouschovias and colleagues do provide an explanation for the core asymmetry, and also predict a significant steepening of the density profile just outside the boundary of the

supercritical core, with $s = -dln\rho/dlnr$ reaching a value as large as $s = 4.4$ in some cases (see Fig. 8 of BM95). In particular, the more subcritical the cloud is initially, the more pronounced this edge is. We note that the steepening of the density profile is significant in the models only after the formation of a supercritical core. Thus, the tentative edge we observe in the north-south direction is in agreement with the magnetic field strength calculations of Section 3.2.2 above in suggesting that L1689B may have just entered the dynamical phase of contraction.

4. Conclusions

Based on our new 1.3 mm continuum maps of L1689B, taken at the IRAM 30-m telescope with the MPIfR bolometer arrays, we confirm that the radial density profile of this pre-stellar core flattens out near its center. Assuming uniform dust properties through the source, the derived density profile of L1689B approaches $\rho(r) \propto r^{-2}$ between $\sim$ 4000 AU and $\sim$ 15000 AU, but is as flat as $\rho(r) \propto r^{-0.4}$ or $\rho(r) \propto r^{-1.2}$ (depending on the deprojection hypothesis) at radii less than $\sim$ 4000 AU (Fig. 5). The mass and density of the relatively flat central region are estimated to be $\sim 0.33\ M_\odot$ and $\sim 2 \times 10^5$ cm^{-3}, respectively. The characteristics of this central region are satisfactorily accounted for by ambipolar-diffusion models of (initially) magnetically-supported, self-gravitating clouds (e.g., Mouschovias 1991) if the mean, central magnetic field is $\lesssim 80\ \mu$G. Although such a high magnetic field has not yet been detected, it is comparable to the field strength inferred by assuming equipartition between the magnetic energy density and the (measured) nonthermal kinetic energy density of the core. Direct, high angular resolution Zeeman measurements of the magnetic field in the dense molecular gas, such as those existing for the B1 core in Perseus (see Crutcher et al. 1994), should be attempted in the case of L1689B to confirm the above interpretation. If indeed supported by a primarily static, nearly uniform magnetic field, L1689B must be close to critical and on the verge of forming one or more protostars of total mass $\sim$ 0.3–2 $M_\odot$. Alternatively, the observed core structure is also roughly consistent with non-magnetic equilibrium models for thermally supported, self-gravitating condensations interacting with a relatively strong UV radiation field (e.g. Falgarone & Puget 1985). In this case, the temperature is predicted to rise substantially in the outer layers of the core.

Sensitive dust continuum observations with bolometer arrays prove to be a powerful tool to study the density structure of pre-stellar cores and gain insight into the initial conditions of star formation. Although a larger number of cores should be mapped before drawing definitive conclusions, our detailed results on L1689B support the suggestion made by WSHA that flat inner density profiles are a common feature of 'Myers' cores without IRAS sources. In contrast, the radial density profiles observed in IRAS dense cores and protostellar envelopes do *not* show this inner flattening (e.g., Ladd et al. 1991; Motte et al. 1995). Since the starless dense cores detected in the submillimetre continuum have an estimated lifetime of $\sim 10^6$ yr (WSHA) and are thought to be the precursors of isolated low-mass protostars, the (presently poor) statistics suggests that the transition from flat to steep inner density profile occurs on a very short timescale ($\lesssim 10^5$ yr), i.e., well in the phase of dynamical collapse. This is indeed predicted by evolutionary models of magnetically-supported cores (e.g., Ciolek & Mouschovias 1994). One important implication is that the initial conditions for rapid protostellar collapse probably more closely resemble critical self-gravitating polytropes (e.g., Bonnor 1956; Chièze 1987) than singular isothermal spheres (Shu 1977) or singular spheres supported by thermal and nonthermal motions (Myers & Fuller 1992). After the onset of fast dynamical collapse, therefore, the evolution may initially differ from the expansion-wave self-similar solution of Shu (1977), and tend towards this solution only at late times (see also Foster & Chevalier 1993). In particular, the mass infall rate is likely to be strongly time-dependent at the beginning of the main accretion phase (see Henriksen 1994). In agreement with this view, a recent homogeneous CO study of outflow activity around low-mass YSOs suggests that the mass loss rate *and* the mass accretion rate both decline dramatically with time from young Class 0 protostars to more evolved Class I protostars (Bontemps et al. 1996).

Acknowledgements. It is a pleasure to thank Glenn Ciolek for enlightening comments about the intricacies of the magnetic core models. We are grateful to Roberto Neri and Robert Zylka for helpful discussions on bolometer data reduction. We would like to thank the British Council and the French APAPE for financial support for travel in the form of an Alliance grant (ref: PN95.219). PPARC and the ROE are acknowledged for Fellowship funding for DWT.

References

Adams, F.C. 1991, ApJ 382, 544
André, P. 1995, In: G.D. Watt & P.M. Williams (eds.) Circumstellar Matter. Ap&SS 224, 29
André, P., Montmerle, T. 1994, ApJ 420,837
André P., Ward-Thompson D., Barsony M., 1993, ApJ, 406, 122 – AWB93
Basu, S., & Mouschovias, T.Ch. 1995, ApJ, 453, 271 – BM95
Beichman C. A., Myers P. C., Emerson J. P., Harris S., Mathieu R., Benson P. J.,Jennings R. E., 1986, ApJ, 307, 337
Benson P. J., Myers P. C., 1989, ApJS, 71, 89 – BM89
Bertoldi, F., & McKee, C.F. 1992, ApJ, 395, 140
Blitz, L. 1993, Protostars & Planets III, p. 125
Bonnor, W.B. 1956, MNRAS, 116, 351
Bontemps, S. 1996, PhD thesis, University of Paris XI
Bontemps, S., André, P., & Ward-Thompson, D. 1995, A&A, 297, 98

Bontemps, S., André, P., Terebey, S. & Cabrit, S. 1996, A&A, in press
Boss, A.P. 1987, ApJ 319,149
Boss, A.P., & Yorke, H.W. 1995, ApJ 439,L55
Broguière, D., & Neri, R. 1995, NIC bolometer user's guide (IRAM internal report)
Chièze, J.-P. 1987, A&A 171, 225
Chièze, J.-P., & Pineau des Forêts, G. 1987, A&A 183, 98
Chini, R., Krügel, E., Haslam, C.G.T., Kreysa, E., Lemke, R., Reipurth, B., Sievers, A., & Ward-Thompson, D. 1993. A&A, **272**, L5
Ciolek, G.E. 1996, private communication
Ciolek, G.E., & Mouschovias, T.Ch. 1994, ApJ, 425, 142
Ciolek, G.E., & Mouschovias, T.Ch. 1995, ApJ, 454, 194
Crutcher, R.M., Mouschovias, T.Ch., Troland, T.H., & Ciolek, G.E. 1994, ApJ, 427, 839
Draine, B.T., & Lee, H.M. 1984, ApJ, 285, 89
Emerson, D.T., Klein, U., & Haslam, C.G.T. 1979, A&A, 76, 92
Falgarone, E., & Puget, J.-L. 1985, A&A, 142, 157
Falgarone, E., & Puget, J.-L. 1986, A&A, 162, 235
Falgarone, E., Puget, J.-L., & Pérault, M. 1992, A&A, 257, 715
Fiedler, R.A., Mouschovias, T.Ch. 1993, ApJ 415,680
Foster, P.N., Chevalier, R.A. 1993, ApJ 416,303
Goodman, A.A., & Heiles, C. 1994, ApJ, 424, 208
Griffin, M.J., & Orton, G.S. 1993, Icarus, 105, 337
Guélin, M., Zylka, R., Mezger, P.G., Haslam, C.G.T., & Kreysa, E. 1995, A&A, 298, L29
Henning, Th., Michel, B., & Stognienko, R. 1995, Planet. Space Sci. (Special issue: Dust, molecules and backgrounds), 43, 1333
Henriksen, R.N. 1994, in: Montmerle T., Lada C.J., Mirabel I.F., Trân Thanh Vân J. (eds.) The Cold Universe. Editions Frontières, p.241
Kreysa, E. 1992, in: ESA-Symposium on Photon Detectors for Space Instrumentation, Noordwijk, p. 207 (ESA SP-356)
Krügel, E., & Siebenmorgen, R. 1994, A&A, 288, 929
Ladd, E.F., Adams, F.C., Casey, S. et al. 1991, ApJ, 382, 555
Lizano, S., & Shu, F.H. 1987, in; G.E. Morfill & M. Scholer (eds.) Physical Processes in Interstellar Clouds, p. 173
Lizano, S., & Shu, F.H. 1989, ApJ, 342, 834
Loren, R.B. 1989a, ApJ, 338, 902
Loren, R.B. 1989b, ApJ, 338, 925
Motte, F., André, P., Neri, R. 1995, in: Siebenmorgen, R., Kaufl, H.U. (eds.) The Role of Dust in the Formation of Stars. ESO Astrophysics Symposia, in press
Mouschovias, T.Ch. 1991, in The Physics of Star Formation and Early Stellar Evolution, Eds. Lada & Kylafis, p. 449
Mouschovias, T.Ch. 1995, In: The Physics of the Interstellar Medium and Intergalactic Medium, ed. A. Ferrara, C.F. Mc Kee, C. Heiles, & P.R. Shapiro (San Francisco: ASP), Vol. 80, 184
Myers P. C. 1983, ApJ, 270, 105
Myers P. C., Linke, R.A., & Benson P. J., 1983, ApJ, 264, 517 – MLB
Myers P. C., & Fuller, G. 1992, ApJ, 396, 631
Myers P. C., & Goodman, A.A. 1988, ApJ, 329, 392
Myers P. C., & Goodman, A.A. 1991, ApJ, 373, 509
Nakano, N. 1979, PASJ, 31, 697
Preibisch, Th., Ossenkopf, V., Yorke, H.W., & Henning, Th. 1993, A&A, 279, 577
Shu F. 1977, ApJ, 214, 488
Shu, F.H., Adams, F.C., Lizano, S. 1987, ARA&A 25,23
Shu, F., Najita, J., Galli, D., Ostriker, E., & Lizano S. 1993, Protostars & Planets III, p. 3
Vrba, F.J., Strom, S.E., & Strom, K. 1976, AJ, 81, 958
Ward-Thompson, D., Jessop, N. E., 1996, in: 'Changing perceptions of the morphology, dust content and dust to gas ratios in galaxies', ed: Block, D., in press, Kluwer, Dordrecht
Ward-Thompson, D., Scott, P.F., Hills, R.E., & André, P. 1994, MNRAS, 268, 276 (WSHA)

This article was processed by the author using Springer-Verlag LaTeX A&A style file *L-AA* version 3.